Hindawi
Advances in Civil Engineering
Volume 2018, Article ID 8618937, 15 pages
https://doi.org/10.1155/2018/8618937

Research Article

An Analytical Study of Square CFT Columns in Bracing Connection Subjected to Axial Loading

Jianrong Pan,[1,2] **Peng Wang**,[1] **Yanjun Zheng**,[1] **Zhan Wang**,[1,2] **and Deming Liu**[1]

[1]*School of Civil Engineering and Transportation, South China University of Technology, Guangzhou 510641, China*
[2]*State Key Laboratory of Subtropical Building Science, South China University of Technology, Guangzhou 510641, China*

Correspondence should be addressed to Peng Wang; pwang1987@126.com

Received 18 July 2018; Revised 17 October 2018; Accepted 6 November 2018; Published 25 November 2018

Academic Editor: Rosario Montuori

This paper presents the behavior of square concrete-filled tubular (CFT) columns with different penetrating gusset plates under axial load. Load transfer mechanism in the CFT columns including load distribution between gusset plate and core concrete and composite action of the gusset plate and steel tube was investigated. Experimental results showed that the axial load can be transferred from the bottom edge, ribs, and the hole of the gusset plate to core concrete through the bearing mechanism. Adding ribs or a hole on the gusset plate can efficiently facilitate load transmission and improve the composite action. Numerical models were established to determine the distribution of axial forces among members in the square CFT column. Then, revised coefficients of elastic modulus for the square CFT column with the gusset plate were proposed.

1. Introduction

CFT columns have been widely used in high-rise buildings in China due to their superior strength, high stiffness, and good structural stability [1–3]. In addition, the steel tubes act as formwork for casting core concrete, which decreases labor cost during construction. Since remarkable benefits above can be expected in circular CFT columns, square or rectangular CFT columns only show a small increase in axial bearing capacity due to the triaxial stress effect, even for those which have large steel wall thickness. Furthermore, local buckling and bending behavior of steel plates in square or rectangular CFT columns is different from that in circular CFT columns [4, 5].

The composite action is particularly essential in seismic design of CFT columns [6, 7]. Current design codes such as Eurocode 4 [8], AISC Specification [9], and CIDECT [10] provide different approaches to calculate load distribution among column members. However, some connections cannot effectively transmit the applied loads into column members as design. There still lacks a clear understanding of the load transfer mechanism in CFT columns such as the composite action and load distribution between steel and core concrete.

A traditional CFT column connection using internal diaphragms [11, 12] requires full penetration welding around the edge of tubes at each beam-column intersection and beam flanges. It is difficult, expensive, and time-consuming to construct this type of connection. A more convenient and economical beam-brace-column connection was proposed by Macrae et al. [13] and Hassan et al. [14]. In this connection, braces and beams were connected to a vertical gusset plate that penetrates to the circular CFT column and forces transfer solely through friction between concrete and steel and bearing at the bottom of the plate.

Hu et al. [15] and Ramadan et al. [16] analyzed the behavior of CFT-to-bracing connections with gusset plates, considering a wide range of parameters including load ratio of the circular CFT column, thickness of the gusset plate, and effect of cutouts. It was found that increasing the thickness of the gusset plate or introducing cutouts slightly improved ultimate strength of the CFT column, while caused more local bulge on the steel tube below the connection area.

As mentioned above, there were very limited research about the factors affecting braced connection to transfer forces into the concrete and steel in concentrically braced frames (CBF) [13, 14], especially BBC connections with square CFT columns in the CBF system. The current design formulas may not produce connections with expecting capacities. ANSI/AISC-360-16 specifications [9] provide load transfer mechanisms including direct bearing, shear connection, and direct bond interaction. These mechanisms, however, can only be considered separately due to lack of study on their combined effects [17].

Braced-frame connections with square or rectangular CFT columns have showed better adaptability to architecture, but the limitation of study in this area restricts their popularization. In this paper, experiments were conducted on the basis of the simplified model of this kind of connection. Four commonly used penetrating gusset plates were chose in experiments. The connections behavior was discussed, the composite action of each specimen was evaluated, the mechanical performance of the braced frame connections with square CFT columns was studied. A finite element model on CFT column specimens was established by using finite element analysis software ABAQUS. Based on the experimental results and the finite element analysis, revised coefficients of elastic modulus for the square CFT column with the gusset plate were proposed.

2. Experimental Program

2.1. Specimens. A common braced frame connection consists of CFT columns, beams, braces, and gusset plates (Figure 1). However, it is difficult to exert load on such complicated connection in the laboratory. A simplified connection is, therefore, proposed in this study. As shown in Figure 1, the loads transferred from both upper and lower braces can be composed to a vertical one applied on the CFT column through the gusset plate. This simplification was demonstrated to be effective by Macrae et al. [13].

Eight square CFT column specimens were prepared according to ANSI/AISC 360-16 [18]. The specimens were divided into four groups according to types of gusset plates as follows: 1, the gusset plate with a thickness of 12 mm; 2, the gusset plate with a thickness of 18 mm; 3, the gusset plate with a circular hole at the center; and 4, the gusset plate with three pairs of solid square ribs. In each group, there are two specimens subject to axial load applied by a flat loading head (SJ1) and a stiffened one (SJ2), respectively (Table 1). Dimension of gusset plates is shown in Figure 3. The column specimens adopted were 1000 mm in height and 400 mm in width. There was a pair of slots with a depth of 400 mm and a width of 2 mm cut in the steel tube. The gusset plate was embedded in the slots by 400 mm and welded on the external surface of the steel tube using 8 mm fillet welds (Figure 4). Mechanical properties of the steel tube and gusset plate are given in Table 2.

2.2. Experimental Setup. In experimental, an axial load was imposed on the loading head by a 1500 t hydraulic jack as shown in Figure 2. The objective of the experiment is to determine the effectiveness of each kind of the gusset plate in transferring forces to the concrete infill and to the tube and find out the level of composite action for each connection type. Two groups of experiment with four specimens in each were designed and built as illustrated in Table 1, the difference between two groups of specimens was the constructions of the loading head plate, and a flat plate that was set as the loading head was placed on the gusset plate to transfer the axial pressure from the hydraulic jack in group SJ1 as shown in Figure 2(b). And a stiffened chuck was adopted to prevent the premature instability in the gusset plate in group SJ2 as shown in Figure 2(c). Therefore, the results of these two groups of experiments can be validated by each other.

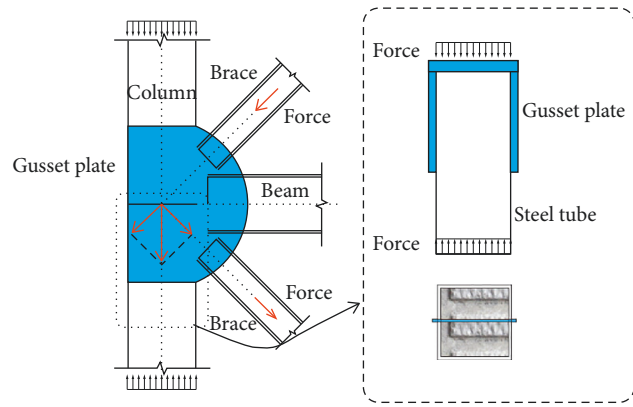

Figure 1: Simple CFT connection in CBF.

Axial load was applied on the top of the gusset plate of column specimens by a 1500 t hydraulic jack (Figure 2(a)). Two different loading heads, flat plate, and stiffened chuck were adopted (Figures 2(b) and 2(c)). Effect of premature instability of the gusset plate on load transfer was studied. Relative slippage between steel tube and core concrete was measured by displacement instruments installed on the top of the steel tube and concrete. Strain gauges were attached on the center line of the gusset plate and tube wall (Figures 3 and 4).

Monotonic axial load was applied by 100 kN each step until the gusset plate yielded. Then, the load was added by 50 kN each step and terminated when out-of-plane buckling occurred at the gusset plate. In each step, the load stayed for two minutes.

3. Analysis of Test Phenomena and Results

3.1. Failure Patterns. The applied load from the top of the gusset plate was transferred to the steel tube through welds and to the concrete by means of bearing and friction. Failure patterns of specimens are shown in Figure 5. Slippage between core concrete and steel tube (Figure 5(a)), plastic deformation, and out-of-plane buckling of the top gusset plate (Figure 5(b)) and lateral expansion of the steel tube (Figure 5(b)) were observed.

Specimens SJ1-1 and SJ1-4 were vertically split up after the test. Core concrete of both specimens shows little

Table 1: Details of the steel tube and gusset plate.

Specimens	Dimension of the steel tube (mm)	Thickness of the gusset plate (mm)	Details of the gusset plate
SJ1-1/SJ2-1	400 × 10 × 400	12	Flat
SJ1-2/SJ2-2	400 × 10 × 400	18	Flat
SJ1-3/SJ2-3	400 × 10 × 400	12	Single hole:
SJ1-4/SJ2-4	400 × 10 × 400	12	Three pairs of solid square ribs

Table 2: Mechanical properties of the steel tube and gusset plate.

Steel parts	Thickness, t (mm)	Yield stress, f_y (MPa)	Ultimate stress, f_u (MPa)	Elasticity modulus, E_s (10^5 MPa)
Plate 18 mm	17.92	400	550	2.07
Plate 12 mm	11.59	440	580	1.88
Tube	9.49	440	580	1.89

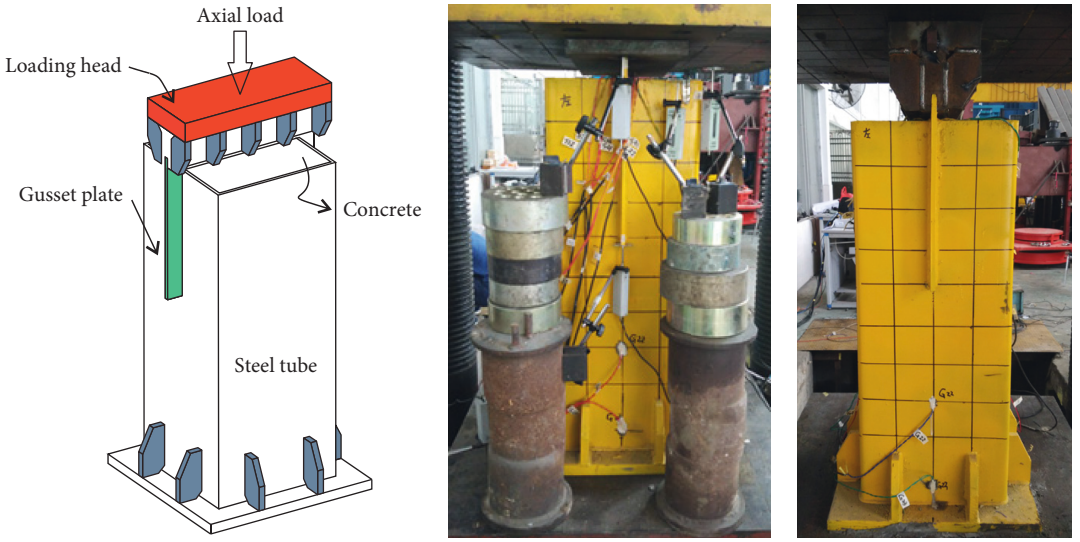

Figure 2: Experimental setup: (a) schematic diagram of the experiment, (b) flat loading head, and (c) stiffened loading head.

damage, except some cracks near the bottom of the gusset plate and below the first rib (Figure 6). Crack width of core concrete was less than 0.1 mm, which is attributed to confinement provided by the steel tube.

3.2. Loading Capacity. Axial load-displacement relationships of specimens are shown in Figure 7. Pattern of the gusset plate exert a significant influence on performance of column specimens under axial load. The gusset plates with a thickness of 18 mm carried the highest load, followed by those with ribs and a thickness of 12 mm, and those with the single hole performed the worst. Both thick plate and ribs on the plate contributed to load transfer, while the circular hole weakened the gusset plate. Loading head did not affect the performance of gusset plates before their instability Therefore, it can be considered that the stress distribution of SJ1 and SJ2 specimens is basically the same before local buckling of gusset plates.

Yield load and ultimate load of specimens are given in Table 3. The yield load and the ultimate load are defined as the load when the top 50 mm of the gusset plate yields and the maximum load is applied on the gusset plate.

3.3. Stress Distribution of the Gusset Plate. Compressive strain of SJ1 gusset plates was measured by strain gauges placed along the midline of the plates. The strains at load of 1000 kN, 2000 kN, yield load, and ultimate load are showed in Figure 8. The difference between the gauge readings along the plate provided indications for the transmission of load from the plate to core concrete.

For the specimens with a plain gusset plate, SJ1-1 and SJ1-2, axial load mainly transferred from the plate to concrete through a chemical bond and friction before the plate reached its yielding load. The strain curves were relatively smooth with small difference along the height of the gusset plate, which meant only a little amount of load transmitted into the concrete during this stage. When the plates yielded, the strain firstly decreased at the height of 400 mm to 100 mm of the plate and then increased at the bottom 100 mm. It turned out that some forces transferred into the concrete infill through direct bearing between the bottom of the plate and the core concrete.

The stain distribution along the gusset plate of specimen SJ1-3, as shown in Figure 8(c), firstly increased to the maximum value at the height of 300 mm of the plate (i.e., the

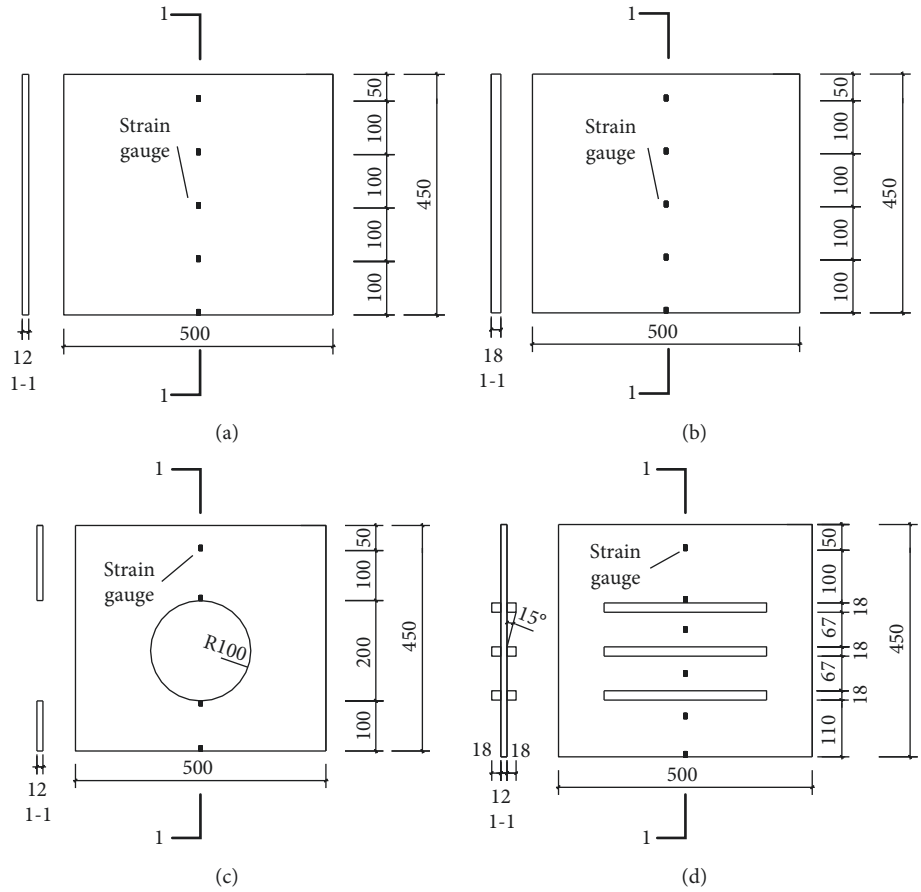

Figure 3: Dimension of the gusset plate and location of the strain gauge: (a) flat: 12 mm; (b) flat: 18 mm; (c) single hole; (d) three pairs of solid square ribs.

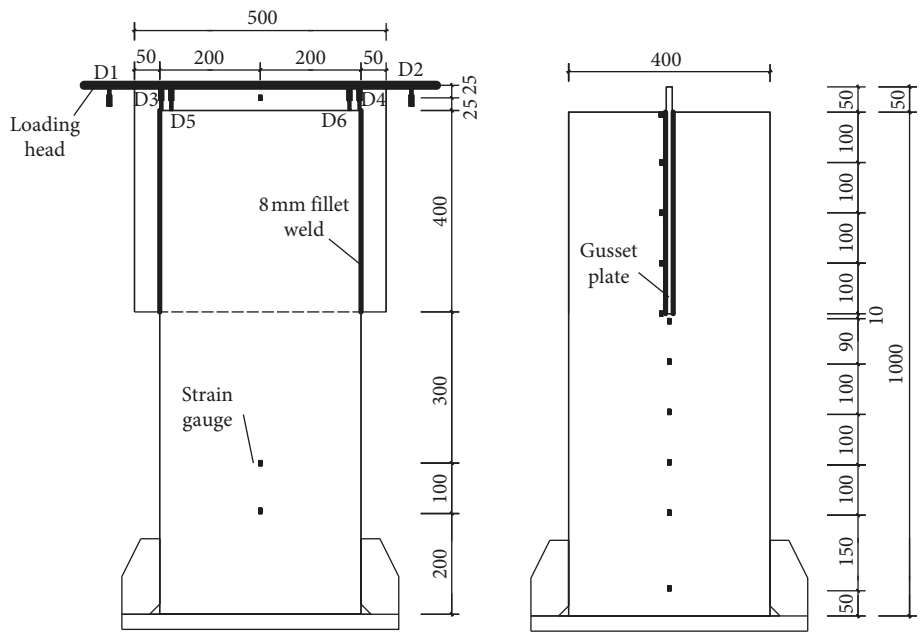

Figure 4: Dimensions of the specimen and location of strain gauge.

(a) (b) (c)

Figure 5: Failure patterns: (a) slippage; (b) buckling in the gusset plate; (c) expansion deformation in the tube.

(a) (b)

Figure 6: Damage in core concrete: (a) SJ1-1; (b) SJ1-4.

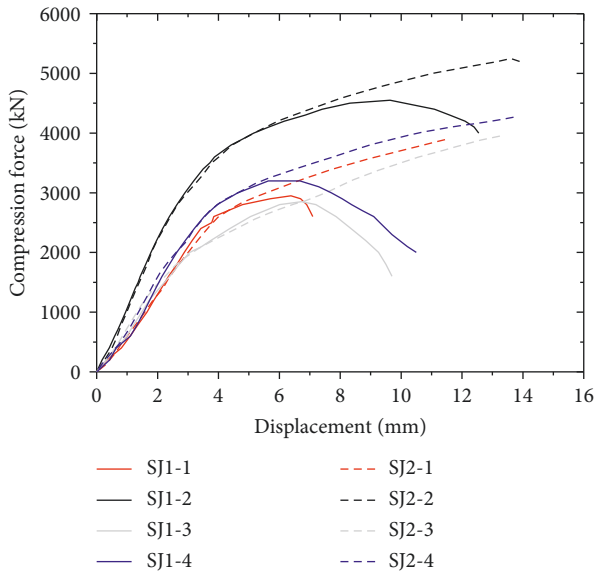

Figure 7: Load curves of the test.

top of the hole). Afterwards, the strain began to decrease sharply from the height of 900 mm to 700 mm (i.e., from the top to the bottom of the hole). The distribution pattern represented that a large amount of load transferred to the concrete through the hole. Furthermore, the strain at the bottom 100 mm of the gusset plate did not increase as that in SJ1-1 and SJ1-2, which meant the force at the bottom of the gusset plate was significantly reduced.

For specimen SJ1-4 with three pairs of ribs welded on the plate, the strain above the ribs slightly differed from that below the ribs at the load of 1000 kN. It was caused by the initial slippage between the steel tube and concrete. This difference between the strain values above and below the ribs shapely enlarged with the increasing load. And the higher demands activated the top rib and allowed the forces to be transferred from the plate into the concrete.

3.4. Strain of the Steel Tube. The strain distributions along the tubes, as seen in Figure 9, differed from each other from the height of 900 mm to 620 mm due to different details of the gusset plate. At the height of 900 mm, the strains of the steel tube in SJ1-2, SJ1-3, and SJ1-4 reached a peak and then decreased along the height of 900 mm to 620 mm, indicating that the partial load was transferred from the tube to the

Table 3: The main results of the tests.

Specimens	Description	Yield load, F_y (kN)	Δ_y (mm)	Ultimate load, F_u (kN)	Δ_u (mm)
SJ1-1	Gusset plate (12 mm)	2500	3.78	2950	7.10
SJ2-1		2500	3.81	3900	11.52
SJ1-2	Gusset plate (18 mm)	3500	3.72	4550	12.55
SJ2-2		3500	3.78	5250	13.90
SJ1-3	Single hole	2100	6.73	2850	9.7
SJ2-3		2100	6.78	3950	13.25
SJ1-4	Ribs	2600	3.53	3200	10.50
SJ2-4		2600	3.55	4300	14.07

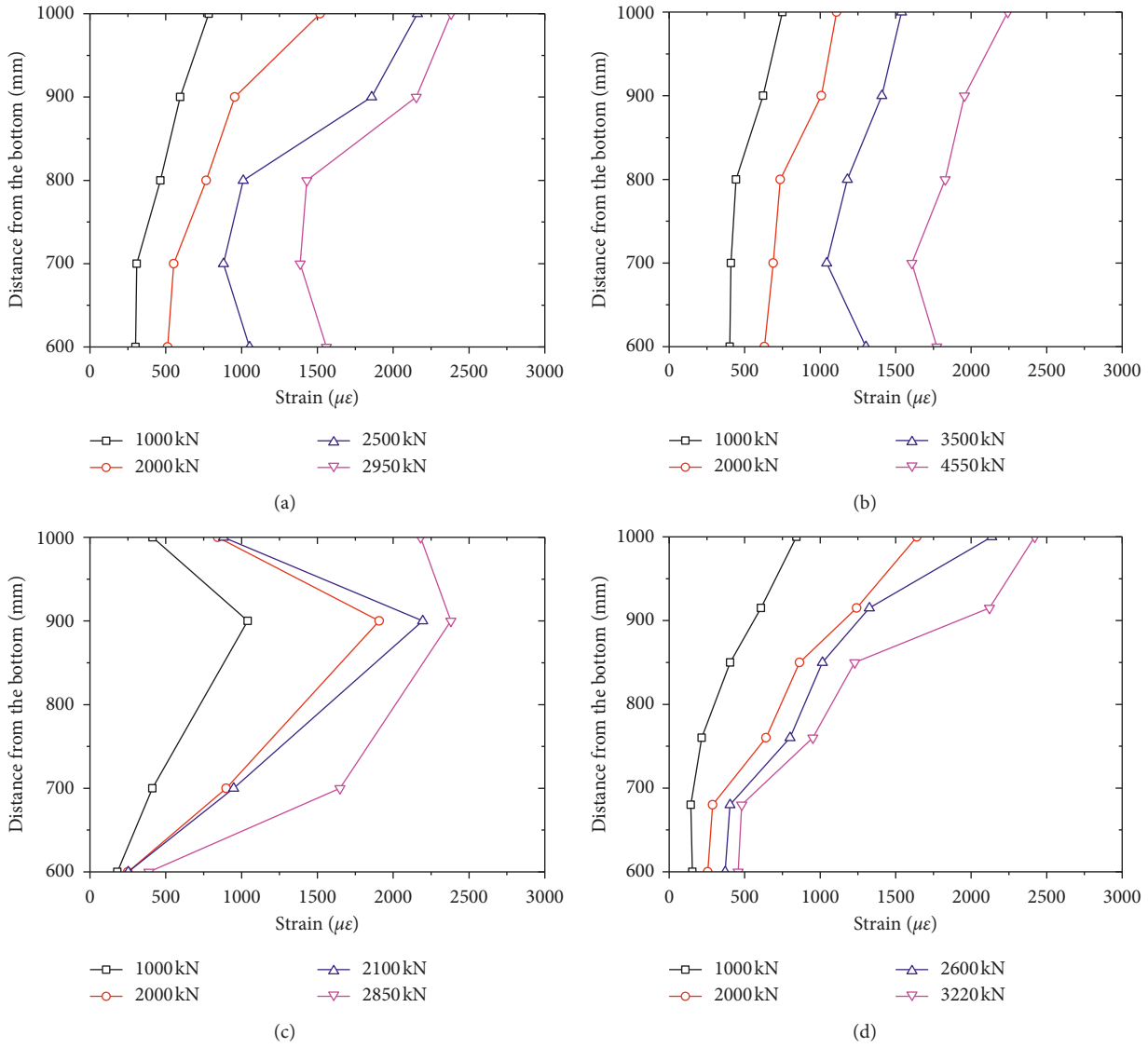

Figure 8: Strain distribution along the gusset plate: (a) SJ1-1; (b) SJ1-2; (c) SJ1-3; (d) SJ1-4.

concrete during this height range. The strain at the height of 580 mm of all specimens, just under the gusset plate, reached another peak because of the direct bearing between the plate and the steel tube. Then, the strain showed a continuous decrease to the base of the tube. This was caused by a chemical bond and friction between the steel tube and core concrete.

At the load of 1000 kN and 2000 kN, the strain distributions along the tubes were similar for all specimens. While at the yield load and the ultimate load, a sharp increase in strain along the tube of specimen SJ1-2 was observed (Figure 9(b)). This can be explained by the local yielding of the steel tube along the welds. The stains of the tube of specimen SJ1-3 significantly reduced at the ultimate loading

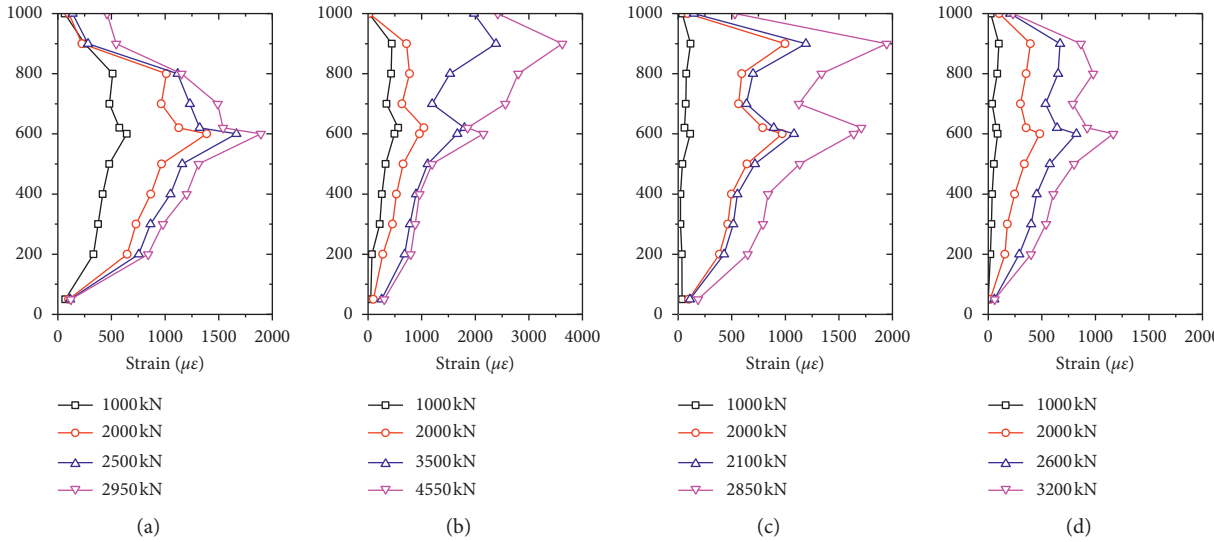

Figure 9: Strain distribution along the steel tube: (a) SJ1-1; (b) SJ1-2; (c) SJ1-3; (d) SJ1-4.

degree at the height from 900 mm to 700 mm where there was an opening on the gusset plate. The strain of the tube of SJ1-4 was much lower than that of SJ1-1, which was benefited by more transfer bearing area on the plate resulted from the ribs in the former. Moreover, the strain of the steel tube in SJ1-4 below the gusset plate was lower than that of SJ1-1. All patterns above reflected a better composite action of specimen SJ1-4.

3.5. Relative Slippage of the Steel Tube and Concrete. The relative slippage between core concrete and the square steel tube can be used to indicate the composite performance for each specimen. An effective gusset plate can minimize the slippage and increase the composite action level. The slippage between steel tube and core concrete is shown in Figure 10.

The slippage of all specimens was negligible below 500 kN. When the load exceeded 500 kN, a chemical bond between the concrete and steel tube broke down, and friction began to control the slippage. The slippage raised with the increasing load. Then, the mechanical transfer mechanisms such as bearing began to take over after approximately 1000 kN. The tendency of slippage with load was approximately linear in all stages.

The specimen SJ1-4 with ribs on the gusset plate exhibited the lowest slippages of 0.185 mm, which was 46% lower than that of SJ1-1. This is because the ribs provide an increase in area 6 times of a plain plate and can interlock concrete and steel together. The slippage of specimen SJ1-3 was reduced by 14% as compared with that of SJ1-1, which indicated that the hole in the center of the gusset plate was also helpful for increasing the bearing area.

4. Finite Element Analysis

4.1. Establishment of the Finite Element Model. To simulate the performance of the CFT column in bracing connection

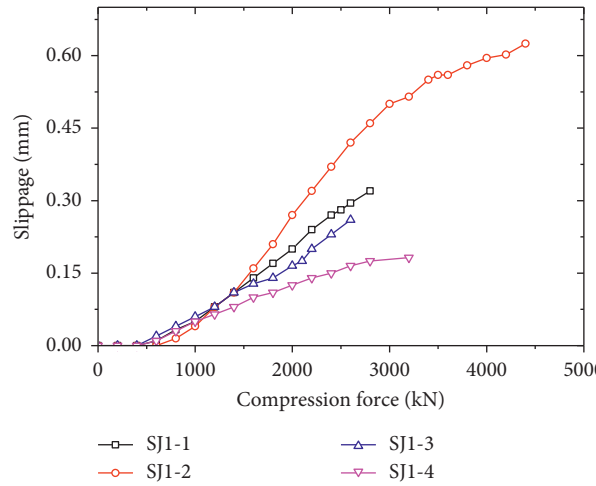

Figure 10: Slippage between the steel tube and concrete core.

with the gusset plate, a finite element analysis model was developed using the ABAQUS/Standard. The model of the simplified connection specimens SJ1-1 was shown in Figure 11, and other models were similar. The boundary condition was set according to the experiment setup, and the bottom of the column was fixed. A coupling constraint was built at the top surface of the gusset plate to apply the displacement control mode in the simulation.

The entire model (steel tube, concrete, gusset plate, and ribs) was modeled using C3D8R elements. The whole model was divided with a structural mesh, and the grid size of the plane was 20 mm, but at least three layers are arranged along the thickness direction of the plate thickness.

A surface-to-surface contact which considers the tangential behavior and normal behavior was established between steel and concrete, and the friction coefficient of the interface between the steel and concrete was 0.6. The gusset plate and steel tube were merged together based on the fact that there is no damage found in the fillet welds between the

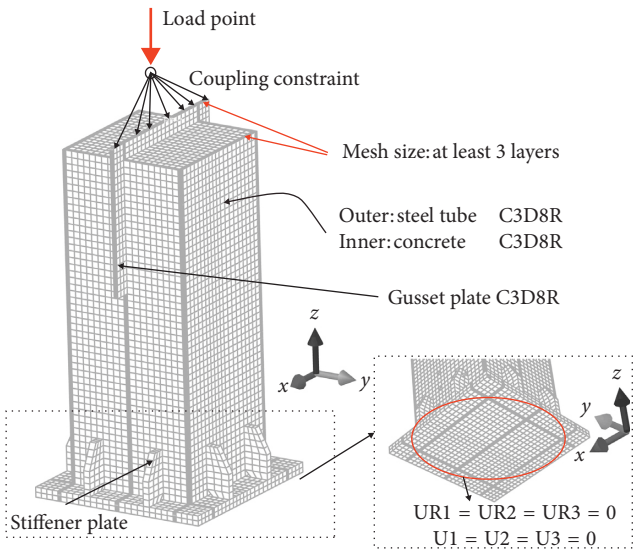

Figure 11: Finite element model.

gusset plate and the steel tube during the test. The solution technique of the simulation was Newton–Raphson (full-Newton as designated in ABAQUS). The convergence criterion for residual force for this nonlinear problem is assumed to be 5×10^{-3} lb.

4.2. Constitutive Relations. The yield strength (f_y) and the ultimate strength (f_u) of the steel measured in the tensile test were adopted, as summarized in Table 1. Poisson's ratio was 0.3. An elastic-plastic model consisting of three stages is used to describe the mechanical behavior of the steel material. A concrete damage plasticity model in software is adopted to simulate the concrete material. The confined effect for concrete is considered in the damage plasticity model but insufficient for experimental CFT columns, and therefore, it is modified by increasing peak strain and transforming descending branch of the input stress-strain curve according to Han et al. [19].

4.3. Results and Analysis

4.3.1. Comparison of Stress Nephograms. Mises stress nephograms of the gusset plates under ultimate load are shown in Figure 12. The stress distribution of specimens had similar patterns. The stress was high near the loading place, while low away from the loading end.

The yielding area at two corners of SJ1-1 and SJ1-2 extends much more than those of SJ1-3 and SJ1-4. Serious stress concentration appeared at the connection part between SJ1-2 and the steel tube. Except the upper corner, there was the yielding part located above and at both side of the opening of the gusset plate of SJ1-3. The stress value below the opening decreased inward and downward. Yielding area of SJ1-4 largely distributed above the first rib because its ultimate load was large. The stress value below ribs was in stepped variation and declined fast.

4.3.2. Cross-Sectional Axial Force Comparison. The internal force transmission and distribution patterns were analyzed in this section. In the finite element analyses, the force transfer patterns could be more directly shown through the analysis in the axial force distribution patterns among different members of the CFT column. Along the height of the steel tube wall, the position of each cross section was corresponded with the arrangement of the strain gauge and the values of the external load were selected as 1000 kN, 2000 kN, yield load, and maximum load. The sum of the axial forces of the gusset plate, the steel tube, and the concrete in each section would be same as the external load.

Variation of axial force with the height of the steel tube is shown in Figure 13. In the height range of the gusset plate, the axial load was transferred through welding connection, and the axial force continuously increased. At the height of the 600 ± 20 mm region, the axial force in the steel tube had a more significant increase due to direct compression between bottom of the gusset plate and the steel tube. Underneath the gusset plate, the axial force varied slightly. Under the same external load, the steel tube of SJ1-1 and SJ1-4 carried the maximum and the minimum axial force, respectively. This phenomenon was also reflected in the slope of height-axial force curves in the height region of the gusset plate, which illustrates core concrete in SJ1-4 carried more external load.

Different from that in the steel tube, axial force was transferred to core concrete mainly through bond and friction between concrete and steel, as well as the contact between concrete and the bottom of the gusset plate. Different details of the gusset plate would lead to different patterns of force variation. Variation of axial force with the height of core concrete is shown in Figure 14. SJ1-1 and SJ1-2 had similar patterns that the axial force of the concrete section slightly increased in the height range of the gusset plate. This is because axial force was transmitted to the concrete mainly through the friction between steel tube and concrete and between gusset plate and concrete in that range. In the area of 600 ± 20 mm in height, the axial force of concrete increased significantly, and this part of the axial force was mainly transferred through the bearing pressure from the gusset plate. The curve of SJ1-3 showed that axial force in the concrete had an obvious increase within the height of the opening of the gusset plate. In the area of 600 ± 20 mm in height, the axial force of concrete of SJ1-3 also increased, but less than that of SJ1-1, which indicated that the opening would improve the force transmission efficiency. Axial force in concrete of SJ1-4 also increased significantly in the height range of the gusset plate, which is attributed to the ribs in force transmission, especially the ribs in the first row. In the area of 600 ± 20 mm in height, the axial force of concrete also increased, but smaller than that in the other specimens. It could be because the ribs on the gusset plate of SJ1-4 have transferred most of load.

The distributions of the internal forces at selected cross section of the gusset plate, concrete, and steel tube and the location of the selected sections are shown in Figures 15 and 16.

For SJ1-1, the axial force of concrete in the section P4 accounted for 27.5% of the total axial force, an increase of

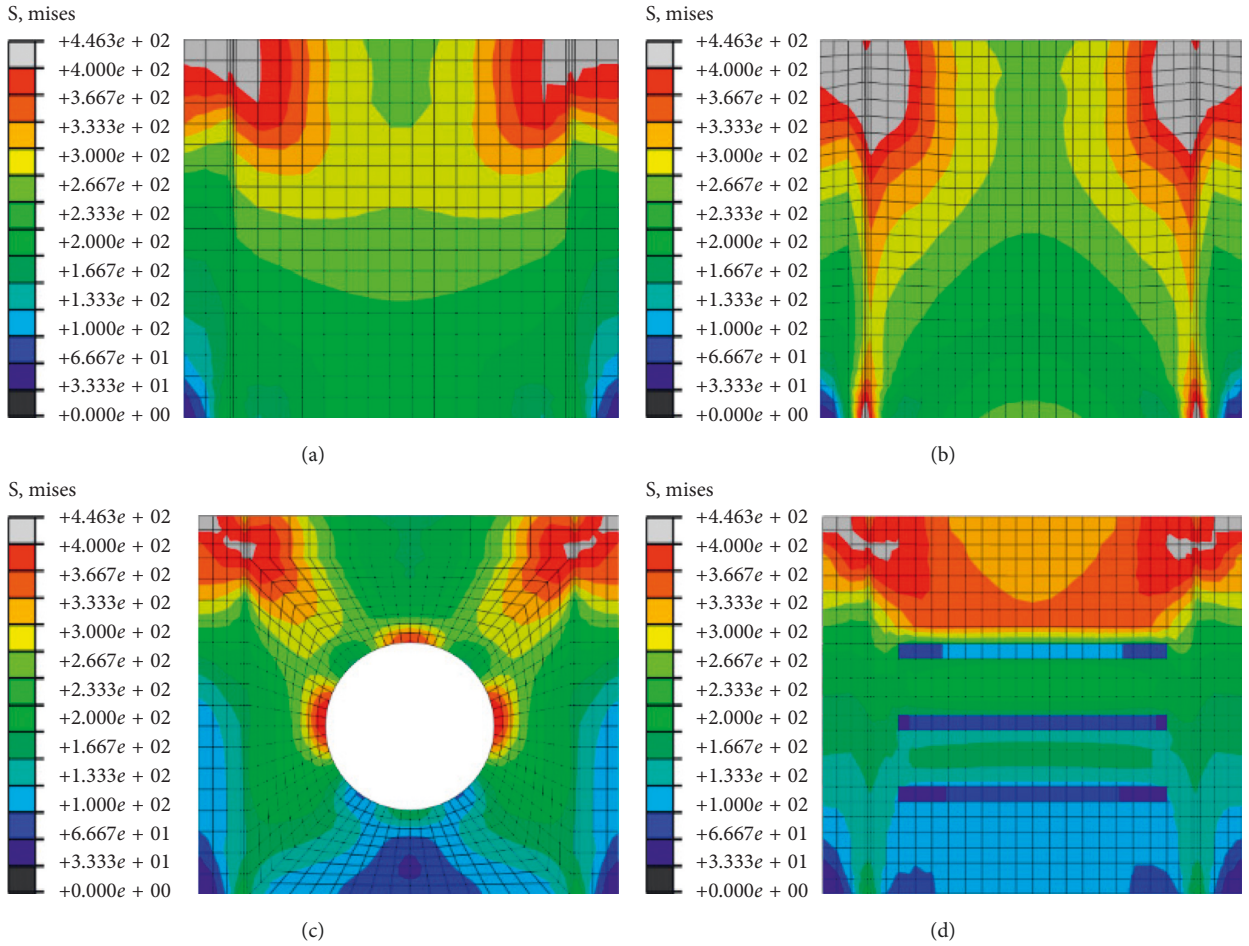

Figure 12: Stress analysis of the plate: (a) SJ-1, (b) SJ-2, (c) SJ-3, (d) SJ-4.

23% compared with that of 4.6% in section P5. If ignoring the bonding effect between sections P4 and P5, this means 23% of the total load could be transferred to concrete through the bottom of the gusset plate because the bonding effect between sections P4 and P5 is negligible. SJ1-2 exhibited similar variation in axial force at a different section with SJ1-1. The axial force at the section P4 increased by 21% compared with that at the section P5. The above analysis showed that increasing the thickness of the gusset plate would increase the pressure between gusset plate and concrete to some extent. For SJ1-3, the axial force of concrete in section P4 was 33.3% of the total axial force, which was 12% higher than that of section P5. The axial force of the section P6 was 21.3%, which showed an increase of 14% over that of the section P7. This showed that 12% and 14% of the total load transferred to the concrete through the opening and the bottom of the gusset plate, respectively. The axial compression at the bottom section of the concrete in SJ1-3 was 36%, which was 20% higher than that in SJ1-1. Compared to that in SJ1-1, axial force in the height of the gusset plate in SJ1-3 was significantly higher, which demonstrates that the gusset plate with opening in center can effectively utilize the concrete in the height of the plate. For SJ1-4, the axial force at the section P4 accounted for 50.5% of the total cross section axial force, which was 14% higher than that at the section P5. According to the analyses results, it could be seen that the internal forces transmitted by the bonding mechanism was about 20% to 30% of the total load, and about 50% of concrete's axial force was from the pressure between the ribs and concrete. The axial compression at the bottom section of concrete in SJ1-4 was 50.7%, which is 68% higher than that in SJ1-1. This indicated that ribs were the most effective way to transfer external load to core concrete.

5. Calculation of Connection Combination

5.1. Combination Level. The amount of the composite action of a specimen is described by the percentage of the composite action, G_{pc}, which is computed according to equation (1), where ε_{gauge} is the strain of the square steel tube measured in experiment, ε_s is the strain of the steel tube carried load independently, and ε_s is calculated as $P/(A_{tube}\ E_{steel})$, where A_{tube} is the cross section area of the tube, E_{steel} is the elastic modulus of the steel, 189 GPa, and P is the axial load on the test specimen. When steel tube and concrete are fully composite, ε_{comp} is computed according to equation (2), where A_{conc} is the area of concrete in the tube and E_{conc} is the elastic modulus of concrete. Moreover, when ε_{gauge} is equal to ε_{steel}, the steel carries all of load and G_{pc} is equal to 0. On the contrary, when ε_{gauge} is equal to ε_{comp}, G_{pc} is equal to

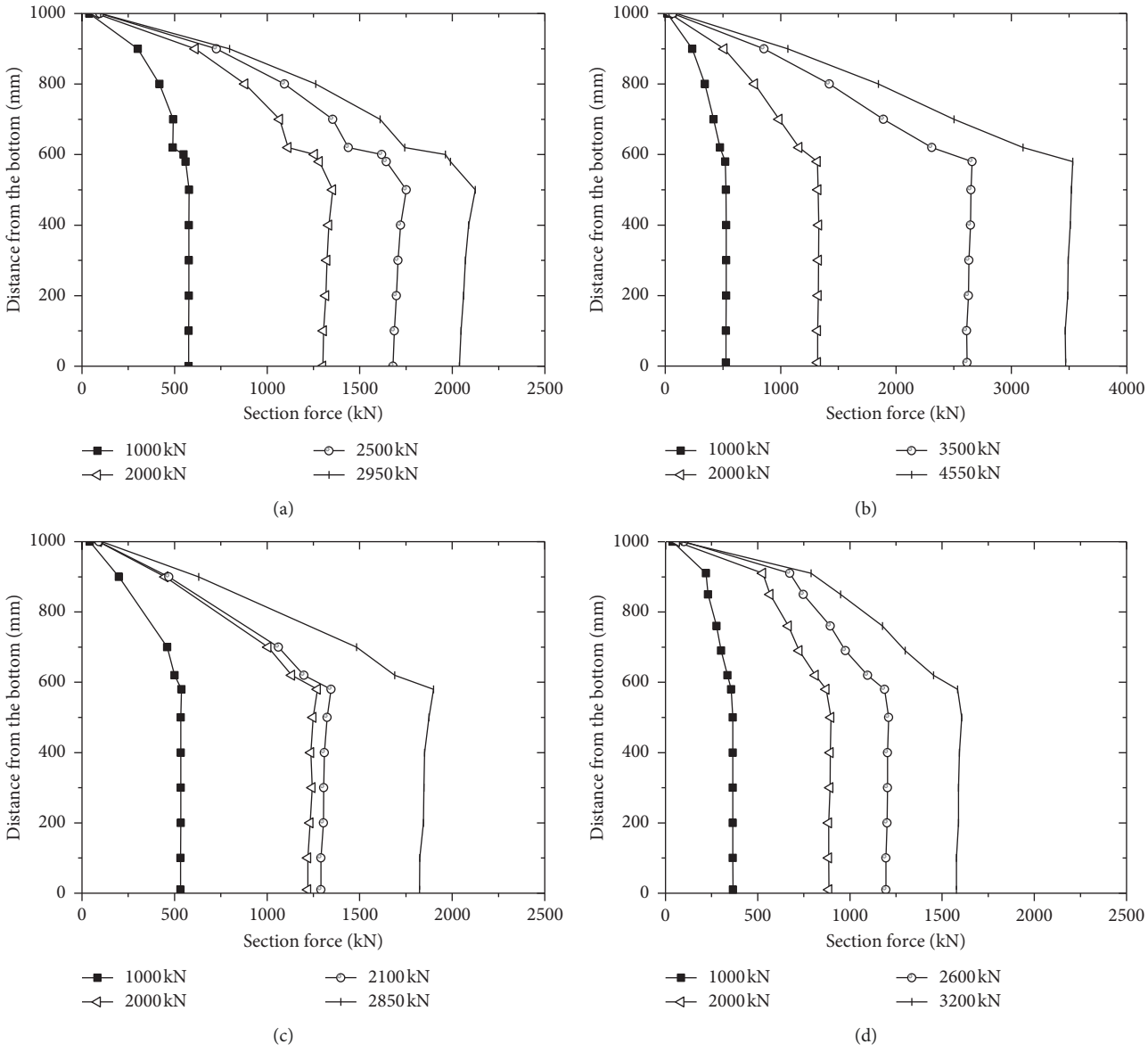

Figure 13: Height-axial force variation curves of steel tube section: (a) SJ-1; (b) SJ-2; (c) SJ-3; (d) SJ-4.

100%. The composite percentage was initially greater than 100% in some cases because of the initial bond between the steel and concrete:

$$G_{pc} = \frac{\varepsilon_s - \varepsilon_{gauge}}{\varepsilon_s - \varepsilon_{comp}} \times 100\%, \quad (1)$$

$$\varepsilon_{comp} = \frac{P}{A_{tube}E_{steel} + A_{conc}E_{conc}}. \quad (2)$$

The percentage of composite action G_{pc} was calculated in four modes as shown in Figure 3: (a) mode 1: using the strain of the steel tube at 200 mm height from the bottom; (b) mode 2: using the strain of the steel tube at 300 mm height; (c) mode 3: using the strain of concrete at 300 mm height; (d) mode 4: using all strains of the steel tube below the gusset plate along the height. The calculating methods for the four different G_{pc} were referred to Gunderson's study [20]. Since the square steel tubes have never yielded in the parts from bottom to 400 mm in height, the maximum change in strain could be used to establish an average stress. G_{pc} at 200 mm and 300 mm of the steel were close, which indicated little bond between concrete and steel in that part. G_{pc} gained from the concrete stress gauges and from the bottom of the test specimen also indicated similar trends to those results obtained from the steel strain gauges.

The final composite action values for each specimen were obtained by a weighted average of the four methods described above (Table 4). In order to exclude the influence of initial bond between the steel and concrete and focus on the

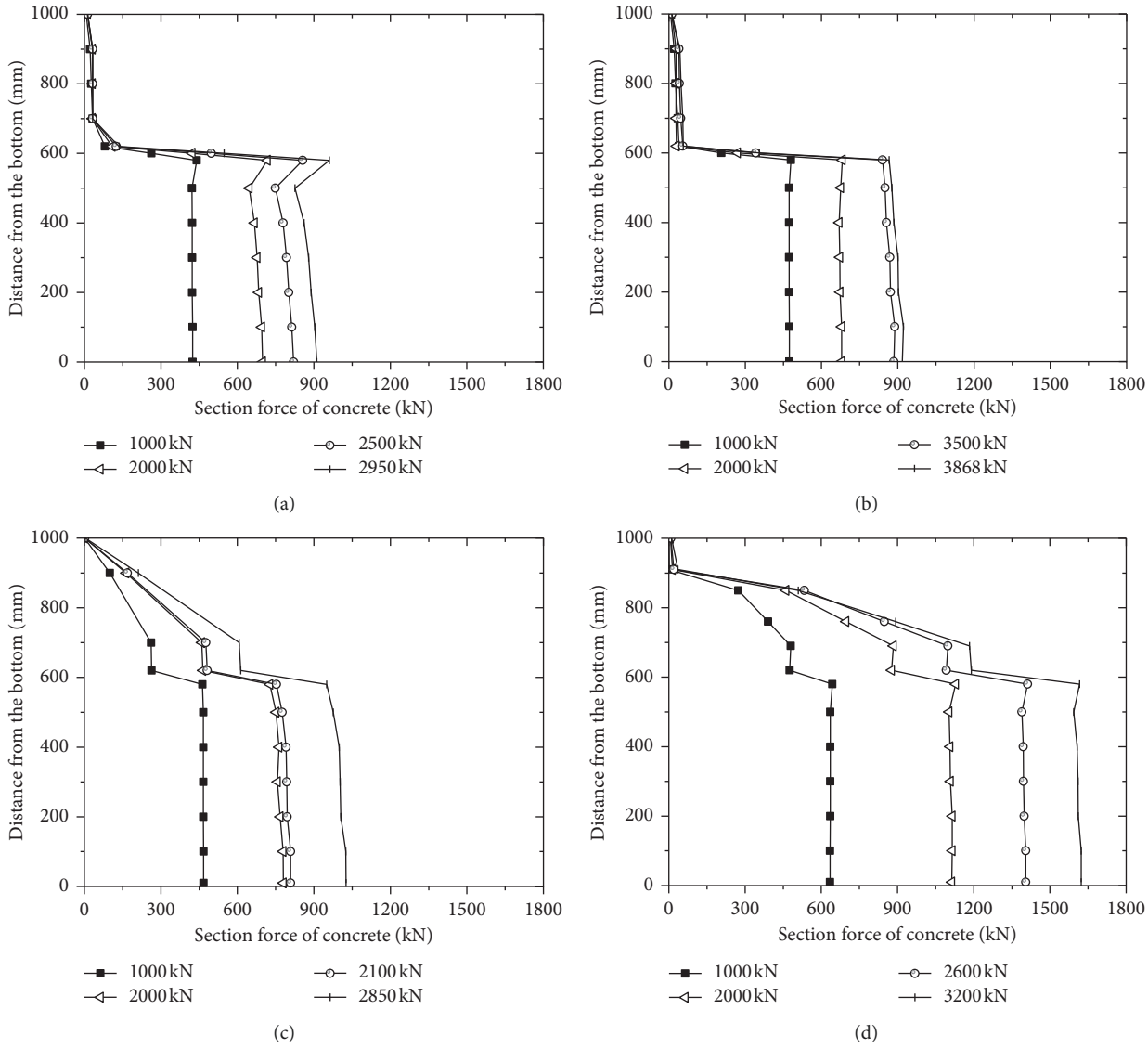

Figure 14: Concrete height-axial force variation curve: (a) SJ-1; (b) SJ-2; (c) SJ-3; (d) SJ-4.

elastic stage considered in engineering design, the average percent of composite action was only calculated from *t* 1000 kN to the yield load.

Composite action of all specimens is shown in Figure 17. The composite degree decreased with increasing load. The initial combined level of specimens was high due to the initial constraint of the interface between the steel tube and the concrete. With the increase of load, there was relative slippage between steel tube and concrete, and the combination level began to decrease. At the end of the loading, the bottom edge, the ribs, and the opening of the gusset plate began to take effect, and more internal force was transferred to the concrete. So the combined effect level remained stable. Specimens with ribs on the gusset plate maintained a high level of combined action throughout. Based on the data of the combination level in Table 4, it can be seen that the combined action level of connections can be improved by increasing the thickness of the gusset plate, using opening or ribs on the gusset plate. The gusset plate with ribs has the highest efficiency for transferring load. The next is the gusset plate with an opening, which increased by 34% as compared with SJ1-1. The combination of the gusset plate was improved slightly by using a thicker gusset plate, which was 12% higher than that of SJ1-1.

5.2. Revised Coefficient of Elastic Modulus. AISC-360-16 [18] chapter E and I2.2 have discussed a composite column under compression, the coefficient "c_e" of elasticity modulus was suggested as 0.4 in prior research [13, 21] representing the concrete's contribution to the stiffness of the entire section, and the coefficient is based on the combination level of steel and concrete. It can be seen from the analyses in this paper that the combined effect level is affected by the types of gusset plates. Therefore, for different gusset plate connections, the elastic modulus coefficient "c_e" is suggested to be corrected by using equation (3). The G_{pc} for calculating the combined level is expressed in the form of equation (4),

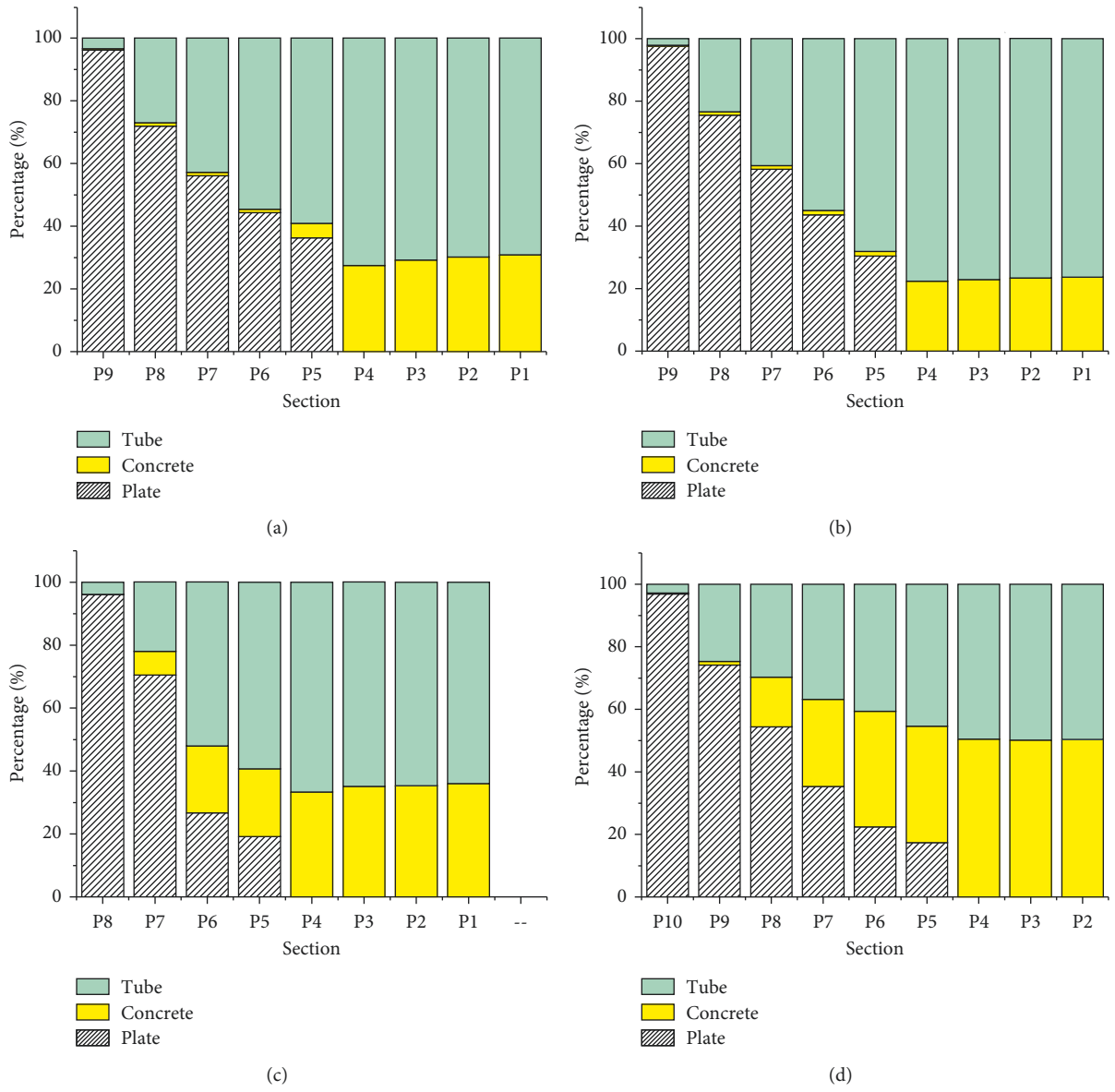

Figure 15: Axial force at different sections: (a) SJ1-1; (b) SJ1-2; (c) SJ1-3; (d) SJ1-4.

where the ratio α of steel tube stiffness and concrete stiffness is calculated from equation (5), so the formula c_e can be calculated as equation (6):

$$E_m = E_s + c_e E_c \left(\frac{A_c}{A_s}\right), \tag{3}$$

$$G_{pc} = \left[\alpha + 1 - \alpha\left(\frac{\alpha + 1}{\alpha + c_e}\right)\right] \times 100\%, \tag{4}$$

$$\alpha = \frac{E_s A_s}{E_c A_c}, \tag{5}$$

$$c_e = \frac{\alpha}{\left((\alpha + 1)/G_{pc}\right) - 1}. \tag{6}$$

Using the formulas above, the composite elastic modulus coefficient of the calculated model is showed in Table 5.

The results showed that the specimen value for the flat gusset plate was closer to 0.4 advised in [21], which verified the accuracy and effectiveness of the calculation equation. For the specimens that had the gusset plate with opening and the gusset plate with ribs, the combined elastic modulus in [21] is conservative. Therefore, it is suggested the combination of the elastic modulus coefficient is 0.4 for the flat gusset plate, 0.5 for the gusset plates with openings, and 0.7 for gusset plates with ribs. Using the modification of the combined elastic modulus coefficient, the capacity of concrete in the CFT column can be fully considered.

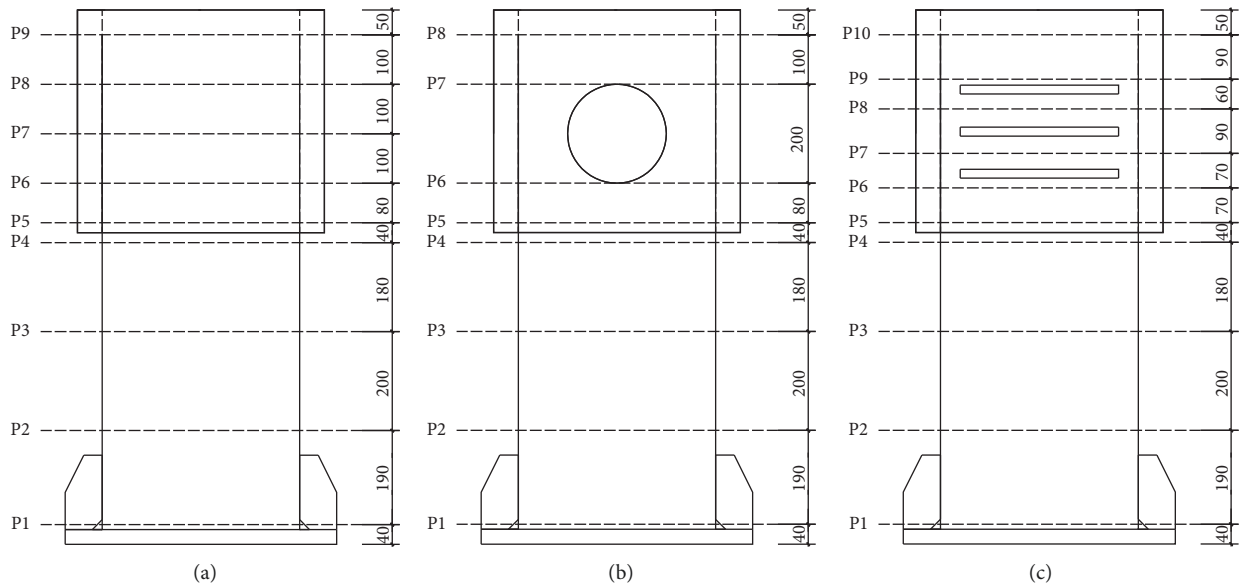

Figure 16: Different cross section along the height of the specimen: (a) SJ1-1/SJ1-2, (b) SJ1-3, (c) SJ1-4.

Table 4: The results of composite action.

Specimens	Mode 1	Mode 2	Mode 3	Mode 4	Average	Average value of the group
SJ1-1	55.40	63.07	36.04	35.52	47.51	49.09
SJ2-1	68.34	65.75	34.36	34.21	50.66	
SJ1-2	60.17	77.19	29.91	51.39	54.66	55.03
SJ2-2	61.40	76.35	36.51	47.36	55.41	
SJ1-3	79.57	85.89	44.78	67.26	69.37	66.92
SJ2-3	76.88	77.33	40.47	63.19	64.47	
SJ1-4	97.16	93.09	52.52	89.00	85.38	86.18
SJ2-4	92.12	97.76	53.51	96.57	86.98	

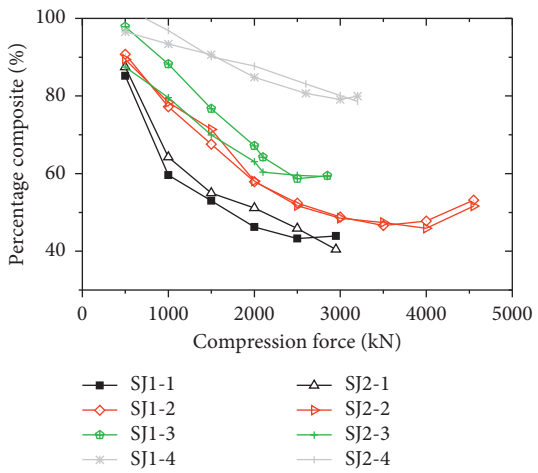

Figure 17: The percentage of composite action.

Table 5: The revised elastic modulus coefficient c_e.

Specimens	Mode 1 c_e	Mode 2 c_e	Average
SJ1-1	0.32	0.4	0.36
SJ2-1	0.45	0.43	0.44
SJ1-2	0.37	0.57	0.47
SJ2-2	0.38	0.55	0.47
SJ1-3	0.6	0.7	0.65
SJ2-3	0.56	0.57	0.57
SJ1-4	0.93	0.84	0.88
SJ2-4	0.82	0.94	0.88

6. Conclusion

In this paper, axial compressive tests were conducted on square CFT columns with different types of gusset plates to study the load transfer mechanism between CFT columns and gusset plates. Finite element analysis was carried out to evaluate the stress distribution in column specimens with the different forms of gusset plates such as the flat gusset plate, gusset plate with opening, and gusset plate with ribs. An amended model to calculate composite action and the elastic modulus coefficient of the CFT column was proposed. Main conclusions of this study are drawn as follows:

(1) A penetrating gusset plate in BBC connection has a good transmission effect. The gusset plate passes the load to the concrete through bond, friction, and the pressure. The load is transferred to the steel tube through the connection of the weld and the vertical pressure between gusset plate and concrete. The

variation curve of the axial force along the height of the gusset plate and the steel tube obtained by the finite element simulation analysis is in good accordance with the height-strain curve of the test.

(2) Increasing the thickness of the gusset plate cannot markedly improve transmission of load to core concrete in the height range of the gusset plate. However, it can improve the transmission in the lower part of the specimen by increasing the bearing area below the gusset plate.

(3) The construction of an opening on the gusset plate can increase the pressure from the plate to concrete core and improve the utilization of the concrete.

(4) The ribs on gusset plates can significantly improve the bearing area and reduce the relative slippage between the concrete and the gusset plate. The plates with ribs perform best in force transmission.

(5) Gusset plate with ribs has the highest composite action, followed by the one with an opening. The combination effect level of using the thicker gusset increase is not obvious.

(6) When the gusset plate is flat, the calculated elasticity combination modulus c_e of the specimen is close to prior research [21], which verifies the accuracy of the combined calculation method proposed in this paper. For the gusset plates with ribs and opening, the elastic modulus coefficient c_e recommended by Galambos [21] is too conservative. It is suggested that the corresponding connection's elastic modulus coefficient could be 0.7 and 0.5, respectively.

Data Availability

The data used to support the findings of this study are available from the corresponding author upon request.

Conflicts of Interest

The authors declare that there are no conflicts of interest.

Acknowledgments

This study was supported by the National Nature Science Foundation of China (51638009 and 51778241), State Key Laboratory of Subtropical Building Science, South China University of Technology (2017ZB28 and 2017KD22), and Fundamental Research Funds for the Central Universities (2017ZD026).

References

[1] A. H. Varma, J. M. Ricles, R. Sause, and L. W. Lu, "Seismic behavior and modeling of high-strength composite concrete-filled steel tube (CFT) beam–columns," *Journal of Constructional Steel Research*, vol. 58, no. 5, pp. 725–758, 2002.

[2] Z. Lai, A. H. Varma, and K. Zhang, "Noncompact and slender rectangular CFT members: experimental database, analysis, and design," *Journal of Constructional Steel Research*, vol. 101, pp. 455–468, 2014.

[3] B. Y. Li, Y. L. Yang, Y. F. Chen et al., "Behavior of connections between square CFST columns and H-section steel beams," *Journal of Constructional Steel Research*, vol. 145, pp. 10–27, 2018.

[4] Y. S. Huang, Y. L. Long, and J. Cai, "Ultimate strength of rectangular concrete-filled steel tubular (CFT) stub columns under axial compression," *Steel and Composite Structures*, vol. 8, no. 2, pp. 115–128, 2008.

[5] R. Montuori and V. Piluso, "Analysis and modelling of CFT members: moment curvature analysis," *Thin-Walled Structures*, vol. 86, no. 1, pp. 157–166, 2015.

[6] C. W. Roeder, G. A. MacRae, C. A. Gunderson, and D. E. Lehman, "Seismic design criteria for CFT braced frame connections," in *Proceedings of 2003 International Workshop on Steel and Concrete, Composite Construction*, Taipei, Taiwan, October 2003.

[7] F. X. Ding, Z. Li, S. Cheng, and Z. W. Yu, "Composite action of hexagonal concrete-filled steel tubular stub columns under axial loading," *Thin Wall Structures*, vol. 107, no. 11, pp. 502–513, 2016.

[8] BS EN 1994-1-1, *Eurocode 4: Design of Composite Steel and Concrete Structures, Part 1-1: General Rules and Rules for Buildings*, British Standards Institution, London, UK, 2004.

[9] AISC/AISC 360-16, *Specification for Structural Steel Buildings*, American Institute of Steel Construction, Inc., Chicago, IL, USA, 2016.

[10] Y. Kurobane, J. A. Packer, J. Wardenier, and N. Yeomans, *Design Guide for Structural Hollow Section Column Connections, CIDECT Design Guide No. 9*, Verlag TÜV Rheinland GmbH, Köln, Germany, 2004.

[11] L. Kang, R. T. Leon, and X. Lu, "Shear strength analyses of internal diaphragm connections to CFT columns," *Steel and Composite Structures*, vol. 18, no. 5, pp. 1083–1101, 2015.

[12] Y. Qin, Z. Chen, J. Bai, and Z. Li, "Test of extended thick-walled through-diaphragm connection to thick-walled CFT column," *Steel and Composite Structures*, vol. 20, no. 1, pp. 1–20, 2016.

[13] G. Macrae, C. W. Roeder, C. Gunderson et al., "Brace-beam-column connections for concentrically braced frames with concrete filled tube columns," *Journal of Structural Engineering*, vol. 130, no. 2, pp. 233–243, 2004.

[14] M. M. Hassan, H. M. Ramadan, M. Naeem, and S. A. Mourad, "Behavior of gusset plate-T0-CCFT connections with different configurations," *Steel and Composite Structures*, vol. 17, no. 5, pp. 735–751, 2014.

[15] H.-T. Hu, C.-W. Chen, and M.-Y. Huang, "Nonlinear finite element analysis of CFT-to-bracing connections subjected to axial compressive forces," *Engineering Structures*, vol. 33, no. 5, pp. 1479–1490, 2011.

[16] H. M. Ramadan, M. M. Hassan, M. A. Mooty, and S. A. Mourad, "Finite element analysis of circular concrete filled tube connections," *Journal of Constructional Steel Research*, vol. 120, pp. 33–44, 2016.

[17] V. W. P. Jacobs and J. F. Hajjar, "Load transfer in composite construction," in *Proceedings of 2010 ASCE/SEI Structures Congress*, Orlando, FL, USA, May 2010.

[18] ANSI/AISC 360-16, *Specification for Structural Steel Buildings*, American Institute of Steel Construction, Chicago, IL, USA, 2016.

[19] L. H. Han, G. H. Yao, and Z. Tao, "Performance of concrete-filled thin-walled steel tubes under pure torsion," *Thin-Walled Structures*, vol. 45, no. 1, pp. 24–36, 2007.

[20] C. A. Gunderson, "Braced frame connections with concrete-filled tube (CFT) columns," Ph.D. thesis, University of Washington, Seattle, WA, USA, 2002.

[21] T. V. Galambos and J. Chapuis, *LRFD Criteria for Composite Columns and Beam Columns, Revised Draft*, Washington University Department of Civil Engineering, St. Louis, MO, USA, 1980.